Available online at www.sciencedirect.com
ScienceDirect
International Journal of Heat and Mass Transfer 51 (2008) 2967–2979
International Journal of HEAT and MASS TRANSFER
www.elsevier.com/locate/ijhmt

Thermal instability of nanofluids in natural convection

D.Y. Tzou *

Department of Mechanical and Aerospace Engineering, University of Missouri-Columbia, Columbia, MO 65211, United States

Received 23 March 2007; received in revised form 10 September 2007
Available online 5 November 2007

Abstract

Thermal (Bénard) instability in nanofluids is investigated in this work. Emphasizing the combined behaviors of Brownian motion and thermophoresis of nanoparticles, the critical Rayleigh number is shown to be lower by one to two orders of magnitude than that for regular fluids. The highly promoted turbulence increases the energy bearing capacity of nanofluids, which could result in higher overall heat transfer coefficient than the increase of the effective thermal conductivity alone. The dominating groups are extracted from the non-dimensional analysis. Close form solutions for the Rayleigh number are derived from the method of eigenfunction expansions and the weighted residual method.

1. Introduction

Nanofluids are mixtures of a regular fluid, such as water or ethylene-glycol, with a very small amount of suspended metallic or metallic oxide nanoparticles (Cu, CuO, Al_2O_3) or nanotubes [1–5]. Typical dimension of the nanoparticles is in the range of a few to about 100 nm. In presence of a mere few percents of nanoparticles, a significant increase of the effective thermal conductivity of nanofluids has been reported. Examples include 40% increase of the effective thermal conductivity in ethylene-glycol nanofluid with 10-nm copper nanoparticles of 0.3% in volume fraction (0.3 vol%) [1] and 10–30% increase of the effective thermal conductivity in alumina/water nanofluids with 1–4 vol% of alumina [5]. Single-phase convective heat transfer coefficient, in parallel, has been extended to estimate the enhancement of the energy bearing capacity of nanofluids. Even with the higher viscosity and effective thermal conductivity accommodated, the Nusselt number for turbulent flow in round tubes can still be over 30% higher than predicted [6–10].

Property changes/enhancements by nanoparticles/nanotubes at extremely low volume fractions are much higher than those expected from the macroscopic models. The governing mechanisms in support of such drastic enhancement in presence of low volume fractions of nanoparticles, as expected, have attracted a lot of attention over the past decade. The surface-area-to-volume ratio inversely proportional to the diameter of the particle is believed to be responsible for the large deviations from the macroscopic model when predicting the effective thermal conductivity [1]. Since most macroscopic model does not include the particle size, the deviation would increase as the particle size becomes smaller. Various attempts have thus been made to determine the governing mechanisms in nanoscale, including a modified Maxwell model accounting for the ordered nanolayer near the particle–fluid interface [11], Brownian motion of nanoparticles in fluids [12,13], ballistic nature of heat transport within nanoparticles [14,15], thermophoretic diffusion of nanoparticles in fluids [10], and thermal lagging in nanoparticles with a large surface-area-to-volume ratio [16]. It seems that combinations of some of above, such as Brownian motion combined with fluid mediated clustering/ballistic phonon transport or thermal lagging combined with large surface-area-to-volume ratios in nanoparticles, contribute much more than

* Tel.: +1 573 882 4060; fax: +1 573 884 5090.
E-mail address: TzouR@missouri.edu

0017-9310/$ - see front matter © 2007 Elsevier Ltd. All rights reserved.
doi:10.1016/j.ijheatmasstransfer.2007.09.014

Nomenclature

a	size parameter of Bénard cell
A, B	coefficient
B	determinant
c	specific heat (J/kg K)
$c_{1,2}$	coefficient
d	diameter of nanoparticles
D	distance (m)
$D_{B,T}$	diffusion coefficient (m^2/s)
f	in-plane distribution of Bènard cell
F	amplitude of volume fraction
g	gravitation (m/s^2)
h	enthalpy (J/kg)
H	parameter
$\mathbf{j}$	mass flux (kg/m^2 s)
k	thermal conductivity (W/m K)
k_B	Boltzmann constant (J/K)
Le	Lewis number
N	ratio
p	pressure (Pa)
P	pressure
Pr	Prandtl number
R_N	N_{TT}/N_{BT}
Ra	Rayleigh number
t	time (s)
T	temperature (K)
u_i	velocity (m/s), $i = 1,2,3$
U_i	velocity, $i = 1,2,3$
x_i	space (m), $i = 1,2,3$
X_i	coordinate, $i = 1,2,3$

Greek symbols

α	thermal diffusivity (m^2/s)
β	thermal expansion coefficient (1/K)
δ	Kronecker delta
ϕ	volume fraction of nanoparticles
Φ	volume fraction
θ	temperature
Θ	temperature amplitude
μ	viscosity (N s/m^2)
ρ	mass density (kg/m^3)
σ	amplification rate of disturbance
τ	time

Subscripts and superscripts

0	reference state, bottom plate
1	top plate
b	bulk
c	critical value
B	Brownian motion
BT	Brownian-to-thermal-diffusivity
f	base fluid
i	imaginary
p	nanoparticle
r	real
T	thermophoresis
TT	thermophoresis-to-thermal-diffusivity
$\bar{z}$	primary flow of z
z'	disturbance of z or dz/dX_3

any effect alone in explaining the anomalous enhancement of the effective thermal conductivity.

Heat transfer enhancement by nanofluid properties (such as the volume-fraction dependent thermal conductivity) has been studied for turbulent force convection [10] and laminar free convection of Newtonian nanofluids [17]. The critical Rayleigh number at the onset of thermal instability that separates the laminar and turbulent regimes, however, has not been made clear, making it difficult in choosing the appropriate correlations in different regimes. The heat transfer coefficient (Nusselt number) of nanofluids remains to be higher in turbulence than that in laminar flow. Promotion of turbulence, in terms of a lower critical Rayleigh number, thus implies an increase of the heat transfer coefficient in the turbulent regime, which may be an equally important source for the overall enhancement of heat transfer. Natural convection plays an important role in the enhancement of the effective thermal conductivity, since the nanoparticles will continuously move in the base fluid due to thermophoresis (movement of nanoparticles from the high temperature site to the low temperature site) and Brownian motion (movement of nanoparticles from the high concentration site to the low concentration site) [10,18]. Even though the nanofluid may appear quiescent over the test section, the internal motion of nanoparticles unavoidably introduces convection into the heat transfer mode. Should natural convection be found more effective in nanofluids, alternatively, the effective thermal conductivity would also be higher since the later is closely related to the overall heat transfer coefficient. While heat transfer correlation for turbulent flow of nanofluids in a round tube has been established [10] and enhancement of thermal conductivity for free convection of nanofluids in a rectangular cavity has been accommodated [19], this work studies the critical Rayleigh number for the onset of Bénard instability in nanofluids. The volume-fraction dependence of nanofluid properties, however, will be temporarily left out and all thermophysical properties of the nanofluids will consequently be assumed constant, due to the recent arguments on the nanoparticle mean free path [20] and the use of new optical beam deflection technique [21] in measuring nanofluid thermal conductivity. In absence of such dependence on the volume fraction, therefore, the emphasis in this work is placed on the significant reduction of the critical Rayleigh number, and hence dominance of turbulence, as a result of the

combined behaviors of Brownian motion and thermophoresis of nanoparticles in stationary fluids. Bènard instability for regular fluids is reformulated to accommodate such effects. It is shown that in presence of a mere 1 vol% of nanoparticles, the critical Rayleigh number, which governs the transition from laminar to turbulent regime, is reduced by *one to two orders of magnitude*. For the nanofluid bounded by a rigid and a free surfaces, the resulting critical Rayleigh number is of the order of several tens (10^1), as compared to 1100.65 (10^3) for regular fluids, which justifies the dominance of turbulence for natural convection in nanofluids. Since the heat transfer rate in turbulence can be higher than that in laminar flow by one order of magnitude, the overall heat transfer coefficient can be significantly higher than that in the regular fluid remaining laminar. To demonstrate such unusual enhancement of turbulence in nanofluids, a nondimensional analysis is performed to extract the dominating parameters and close form solutions are obtained to avoid all numerical uncertainties. Their effects are illustrated along with the characteristic dimension of the Bènard cells at the onset of thermal instability.

2. Formulation

While viscosity, density, thermal conductivity, and specific heat of nanofluids strongly depend on the volume fraction of nanoparticles, for the purpose of characterization and estimates of the various effects on the order of magnitude, all thermophysical properties of nanofluid shall be assumed constant in the analytical formulation. The nanofluid is assumed incompressible, with gravity aligned with the x_3-direction. The continuity and momentum equations are

$$\frac{\partial u_j}{\partial x_j}=0,\quad \rho\left(\frac{\partial u_i}{\partial t}+u_j\frac{\partial u_i}{\partial x_j}\right)=-\frac{\partial p}{\partial x_i}+\mu u_{i,jj}-\rho g\delta_{i3},\quad i,j=1,2,3, \tag{1}$$

where a repeated index (j) refers to summation, $u_j(\partial/\partial x_j)\equiv u_1(\partial/\partial x_1)+u_2(\partial/\partial x_2)+u_3(\partial/\partial x_3)$ and $u_{i,jj}\equiv u_{i,11}+u_{i,22}+u_{i,33}=\nabla^2 u_i$. The nanofluid density (ρ) in Eq. (1) is

$$\rho=\phi\rho_{\rm p}+(1-\phi)\rho_{\rm f},\quad \text{or}\quad \frac{\rho}{\rho_{\rm f}}=\phi\left(\frac{\rho_{\rm p}}{\rho_{\rm f}}\right)+(1-\phi). \tag{2}$$

The density of the nanofluid can be approximated by that of the base fluid, i.e., $\rho\cong\rho_{\rm f}$, since the volumetric fraction of nanoparticles is only a few percent [1]. For alumina nanoparticles in water, for example, $(\rho_{\rm p}/\rho_{\rm f})\cong 4$ and a value of $\phi=2\%$ results in $(\rho/\rho_{\rm f})\cong 1.06$. With the nanofluid density used in Eq. (1), therefore, the Boussinesq approximation is extended to the base fluid ($\rho_{\rm f}$) in accounting for the density change due to the temperature change. The specific weight (ρg) in Eq. (1) thus becomes

$$\rho g=\left[\phi\rho_{\rm p}+(1-\phi)\rho_{\rm f}\right]g\cong\left[\phi\rho_{\rm p}+(1-\phi)\{\rho(1-\beta(T-T_0))\}\right]g. \tag{3}$$

Relative to the flow velocities, nanoparticles also display Brownian motion and thermophoresis due to their size on the nanoscale. Brownian motion is proportional to the volumetric fraction of nanoparticles, in the direction from high to low concentration, whereas the thermophoresis is proportional to the temperature gradient, from hot to cold. Mass flux of the nanoparticles in base fluid ($\mathbf{j}_{\rm p}$), therefore, is superposition of the two [10],

$$\mathbf{j}_{\rm p}=-\rho_{\rm p}D_{\rm B}\nabla\phi-\rho_{\rm p}\left(\frac{D_{\rm T}}{T_{\rm b}}\right)\nabla T, \tag{4}$$

where $D_{\rm B}$ represents the Brownian diffusion coefficient, given by the Einstein–Stokes's equation, and $D_{\rm T}$ represents the thermophoretic diffusion coefficient of the nanoparticles:

$$D_{\rm B}=\frac{k_{\rm B}T}{3\pi\mu d_{\rm p}},\quad D_{\rm T}=\left(\frac{\mu}{\rho}\right)\left(\frac{0.26k}{2k+k_{\rm p}}\right)\phi. \tag{5}$$

Note that the expression $D_{\rm T}$ shown in Eq. (5) was established for particles greater than 1 μm in diameter. In absence of thermophoretic data, however, it has also been extended to particles of mean diameters in 1–100 nm. Vector notations are recovered in Eq. (4) to avoid coexistence of p (for nanoparticles) and j (Cartesian coordinates) in the indicial notations. In the linear theory, temperature change in the nanofluid is small comparing to the bulk temperature ($T_{\rm b}$). Therefore, nanofluid temperature T in the denominator of Eq. (4) has been replaced by $T_{\rm b}$. Assuming constant coefficients in Eq. (4), the continuity equation for the nanoparticles is

$$\frac{\partial\phi}{\partial t}+u_j\frac{\partial\phi}{\partial x_j}=-\frac{1}{\rho_{\rm p}}\nabla\cdot\mathbf{j}_{\rm p}=D_{\rm B}\phi_{,jj}+\left(\frac{D_{\rm T}}{T_{\rm b}}\right)T_{,jj}. \tag{6}$$

Drifting of nanoparticles in fluids represented by $\mathbf{j}_{\rm p}$, now including both Brownian motion and thermophoretic diffusion relative to the flow velocities, introduces additional flow work in the energy equation

$$\rho c\left[\frac{\partial T}{\partial t}+u_j\frac{\partial T}{\partial x_j}\right]=-\nabla\cdot\mathbf{q}+h_{\rm p}\nabla\cdot\mathbf{j}_{\rm p}\quad\text{where}\quad\mathbf{q}=-k\nabla T+h_{\rm p}\mathbf{j}_{\rm p}. \tag{7}$$

Substituting the expression for $\mathbf{q}$ and restoring $\mathbf{j}_{\rm p}$ as shown in Eq. (4), the energy equation becomes

$$\rho c\left[\frac{\partial T}{\partial t}+u_j\frac{\partial T}{\partial x_j}\right]=kT_{,jj}+\rho_{\rm p}c_{\rm p}\left[D_{\rm B}\left(\frac{\partial\phi}{\partial x_j}\right)\left(\frac{\partial T}{\partial x_j}\right)+\left(\frac{D_{\rm T}}{T_{\rm b}}\right)\left|\frac{\partial T}{\partial x_j}\right|^2\right]. \tag{8}$$

Clearly, Brownian motion and thermophoresis of nanoparticles introduce additional nonlinear effects for heat transport in nanofluids.

Eqs. (1), (6), and (8) provide six equations for six unknowns: three velocity components (u_i), pressure (p), volumetric fraction of nanoparticles (ϕ), and temperature (T). Introducing the following nondimensional parameters

$$X_i=\frac{x_i}{D},\quad \tau=\frac{t}{\left(D^2/\alpha\right)},\quad P=\frac{p}{\left(\rho\alpha^2/D^2\right)},\quad \Phi=\frac{\phi-\phi_1}{\phi_0-\phi_1},$$
$$\theta=\frac{T-T_1}{T_0-T_1},\quad U_i=\frac{u_i}{(\alpha/D)}, \tag{9}$$

the unabridged forms of Eqs. (1), (6), and (8) become

$$\frac{\partial U_1}{\partial X_1}+\frac{\partial U_2}{\partial X_2}+\frac{\partial U_3}{\partial X_3}=0, \tag{10}$$
$$\frac{\partial U_1}{\partial \tau}+U_1\frac{\partial U_1}{\partial X_1}+U_2\frac{\partial U_1}{\partial X_2}+U_3\frac{\partial U_1}{\partial X_3}=-\frac{\partial P}{\partial X_1}+Pr\nabla^2U_1, \tag{11}$$
$$\frac{\partial U_2}{\partial \tau}+U_1\frac{\partial U_2}{\partial X_1}+U_2\frac{\partial U_2}{\partial X_2}+U_3\frac{\partial U_2}{\partial X_3}=-\frac{\partial P}{\partial X_2}+Pr\nabla^2U_2, \tag{12}$$
$$\begin{aligned}&\frac{\partial U_3}{\partial \tau}+U_1\frac{\partial U_3}{\partial X_1}+U_2\frac{\partial U_3}{\partial X_2}+U_3\frac{\partial U_3}{\partial X_3}\\&=-\frac{\partial P}{\partial X_3}+Pr\nabla^2U_1-H\left\{[-1+\beta(T_1-T_0)](\phi_1-1)+R_\rho\phi_1\right\}\\&\quad-RaPr(\phi_1-1)\theta-H\left[R_\rho-1+\beta(T_1-T_0)\right](\phi_0-\phi_1)\Phi\\&\quad-RaPr(\phi_0-\phi_1)\theta\Phi,\quad \text{with } H=\frac{RaPr}{\beta(T_0-T_1)},\end{aligned} \tag{13}$$
$$\frac{\partial \Phi}{\partial \tau}+U_1\frac{\partial \Phi}{\partial X_1}+U_2\frac{\partial \Phi}{\partial X_2}+U_3\frac{\partial \Phi}{\partial X_3}=N_{\mathrm{BT}}\nabla^2\Phi+N_{\mathrm{TT}}\nabla^2\theta, \tag{14}$$
$$\begin{aligned}&\frac{\partial \theta}{\partial \tau}+U_1\frac{\partial \theta}{\partial X_1}+U_2\frac{\partial \theta}{\partial X_2}+U_3\frac{\partial \theta}{\partial X_3}\\&=\nabla^2\theta+\frac{1}{Le}\left[\left(\frac{\partial \Phi}{\partial X_1}\right)\left(\frac{\partial \theta}{\partial X_1}\right)+\left(\frac{\partial \Phi}{\partial X_2}\right)\left(\frac{\partial \theta}{\partial X_2}\right)\right.\\&\quad\left.+\left(\frac{\partial \Phi}{\partial X_3}\right)\left(\frac{\partial \theta}{\partial X_3}\right)\right]\\&\quad+\frac{R_{\mathrm{N}}}{Le}\left[\left(\frac{\partial \theta}{\partial X_1}\right)^2+\left(\frac{\partial \theta}{\partial X_2}\right)^2+\left(\frac{\partial \theta}{\partial X_3}\right)^2\right].\end{aligned} \tag{15}$$

The nanofluid is thus characterized by seven parameters:

$$Ra=\frac{gD^3\beta(T_0-T_1)}{\alpha^2}\,(\text{Rayleigh number}),$$
$$Pr=\frac{\nu}{\alpha}\,(\text{Prantdl number}),$$
$$Le=\frac{k}{\rho_{\mathrm{p}}c_{\mathrm{p}}D_{\mathrm{B}}(\phi_0-\phi_1)}\,(\text{Lewis number}),$$
$$N_{\mathrm{BT}}=\frac{D_{\mathrm{B}}}{\alpha},\quad R_\rho=\frac{\rho_{\mathrm{p}}}{\rho},$$
$$N_{\mathrm{TT}}=\frac{D_{\mathrm{T}}}{\alpha}\left(\frac{T_0-T_1}{\phi_0-\phi_1}\right),$$
$$\text{and}\quad R_{\mathrm{N}}=\frac{N_{\mathrm{TT}}}{N_{\mathrm{BT}}}. \tag{16}$$

2.1. Primary flow

Parallel to the Bénard instability for regular fluids [22], Eqs. (10)–(15) will be studied for a quiescent nanofluid between two parallel plates between $x_3=0$ and $x_3=D$, where temperature and volumetric fraction of nanoparticles are kept constant: $T=T_0$ and $\phi=\phi_0$ at $x_3=0$ and $T=T_1$ and $\phi=\phi_1$ at $x_3=D$. In terms of the nondimensional variables defined in Eq. (9), they are $\theta=1$ and $\Phi=1$ at $X_3=0$ and $\theta=0$ and $\Phi=0$ at $X_3=1$.

The primary flow is assumed to be stationary, $\bar{U}_i=0$ for $i=1, 2, 3$, with both temperature ($\bar{\theta}$) and nanoparticle volumetric fraction ($\bar{\Phi}$) varying in the X_3-direction only. From Eqs. (13)–(15), the equations governing the primary flow are thus

$$\begin{aligned}&\frac{\mathrm{d}^2\bar{\Phi}}{\mathrm{d}X_3^2}+R_{\mathrm{N}}\frac{\mathrm{d}^2\bar{\theta}}{\mathrm{d}X_3^2}=0,\\&\frac{\mathrm{d}^2\bar{\theta}}{\mathrm{d}X_3^2}+\frac{1}{Le}\left(\frac{\mathrm{d}\bar{\Phi}}{\mathrm{d}X_3}\right)\left(\frac{\mathrm{d}\bar{\theta}}{\mathrm{d}X_3}\right)+\frac{R_{\mathrm{N}}}{Le}\left(\frac{\mathrm{d}\bar{\theta}}{\mathrm{d}X_3}\right)^2=0,\\&-\frac{\mathrm{d}\bar{P}}{\mathrm{d}X_3}=H\left\{[-1+\beta(T_1-T_0)](\phi_1-1)+R_\rho\phi_1\right\}\\&\qquad+RaPr(\phi_1-1)\bar{\theta}+H\left[R_\rho-1+\beta(T_1-T_0)\right]\\&\qquad\times(\phi_0-\phi_1)\bar{\Phi}+RaPr(\phi_0-\phi_1)\bar{\theta}\bar{\Phi}.\end{aligned} \tag{17}$$

The boundary conditions for $\bar{\theta}(X_3)$ and $\bar{\Phi}(X_3)$ are

$$\bar{\theta}(0)=1,\quad \bar{\Phi}(0)=1\quad\text{and}\quad \bar{\theta}(1)=0,\quad \bar{\Phi}(1)=0. \tag{18}$$

The equations governing $\bar{\theta}$ and $\bar{\Phi}$ in Eq. (17) are nonlinearly coupled, with the relation

$$\bar{\Phi}=-R_{\mathrm{N}}\bar{\theta}+c_1X_3+c_2 \tag{19}$$

followed from the first expression in Eq. (17). Substituting Eq. (19) into the second equation in Eq. (17), it results in

$$\frac{\mathrm{d}^2\bar{\theta}}{\mathrm{d}X_3^2}+\frac{c_1}{Le}\left(\frac{\mathrm{d}\bar{\theta}}{\mathrm{d}X_3}\right)=0, \tag{20}$$

which can easily be integrated for $\bar{\theta}$. Substituting the result of $\bar{\theta}$ into Eq. (19) and employing the boundary conditions in Eq. (18) in the process of integrations, the primary flow is determined:

$$\begin{aligned}\bar{\Phi}(X_3)&=\left\{R_{\mathrm{N}}\exp\left[\frac{(1+R_{\mathrm{N}})X_3}{Le}\right]\right.\\&\quad+\exp\left(\frac{1+R_{\mathrm{N}}}{Le}\right)[1-(1+R_{\mathrm{N}})X_3]\\&\quad\left.+(1+R_{\mathrm{N}})(X_3-1)\right\}\Big/\left[\exp\left(\frac{1+R_{\mathrm{N}}}{Le}\right)-1\right],\\\bar{\theta}(X_3)&=\left\{1-\exp\left[-\frac{(1+R_{\mathrm{N}})(1-X_3)}{Le}\right]\right\}\Big/\\&\quad\left\{1-\exp\left(-\frac{1+R_{\mathrm{N}}}{Le}\right).\right\}\end{aligned} \tag{21}$$

The pressure distribution in the primary flow, $\bar{P}$, can then be obtained by integrating the third expression in Eq. (17) with respect to X_3, with $\bar{\theta}$ and $\bar{\Phi}$ given by Eq. (21). For most nanofluids investigated so far [10], $R_N\sim10^0$–10, $Le\sim10^5$–10^6, and consequently $\varepsilon=(1+R_N)/Le\sim10^{-5}$–$10^{-4}$. Expanding $\bar{\theta}$ and $\bar{\Phi}$ into the power series of ε and retaining up to the first-order terms,

$$\bar{\Phi}(X_3) = 1 - X_3 + \left[\frac{R_N X_3(X_3-1)}{2}\right]\varepsilon + \cdots,$$
$$\bar{\theta}(X_3) = 1 - X_3 + \left[\frac{X_3(1-X_3)}{2}\right]\varepsilon + \cdots \tag{22}$$

with $\varepsilon \sim 10^{-4}$, as compared to $(1 - X_3) \sim 10^0$, the zeroth order terms are dominant in both $\bar{\theta}$ and $\bar{\Phi}$. Consequently, $\bar{\theta}(X_3) = \bar{\Phi}(X_3) \cong 1 - X_3$, which display *linear* distributions in X_3. Nonlinear behaviors in Eq. (21) become pronounced for $Le \sim 10$ and smaller. For the nanofluids being explored so far, however, the value of Lewis number (Le) is about three to four orders of magnitude larger. Even though closed form solutions for $\bar{\theta}$ and $\bar{\Phi}$ exist, therefore, the linear approximations, i.e., $\bar{\theta}(X_3) = \bar{\Phi}(X_3) \cong 1 - X_3$, are adequate and will be used in this work.

2.2. Disturbance flow

Disturbances are now superimposed onto the primary flow,

$$U_i = U_i', \quad P = \bar{P} + P', \quad \theta = \bar{\theta} + \theta', \quad \Phi = \bar{\Phi} + \Phi', \tag{23}$$

with $\bar{\theta} = \bar{\Phi} \cong 1 - X_3$, and consequently $d\bar{\theta}/dX_3 = d\bar{\Phi}/dX_3 = -1$, substitution of Eq. (23) into Eqs. (10)–(15) yields

$$\frac{\partial U_1'}{\partial x_1} + \frac{\partial U_2'}{\partial x_2} + \frac{\partial U_3'}{\partial x_3} = 0 \tag{24}$$

$$\frac{\partial U_1'}{\partial \tau} = -\frac{\partial P'}{\partial x_1} + Pr\nabla^2 U_1', \quad \frac{\partial U_2'}{\partial \tau} = -\frac{\partial P'}{\partial x_2} + Pr\nabla^2 U_2', \tag{25}$$

$$\frac{\partial U_3'}{\partial \tau} = -\frac{\partial P'}{\partial x_3} + Pr\nabla^2 U_3' - RaPr(\phi_1 - 1)\theta' - (\phi_0 - \phi_1)\{H\left[R_\rho - 1 + \beta(T_1 - T_0)\right]\Phi' + RaPr\left(\bar{\theta}\Phi' + \bar{\Phi}\theta'\right)\}, \tag{26}$$

$$\frac{\partial \Phi'}{\partial \tau} - U_3' = N_{BT}\nabla^2\Phi' + N_{TT}\nabla^2\theta', \tag{27}$$

$$\frac{\partial \theta'}{\partial \tau} - U_3' = \nabla^2\theta' - \frac{1}{Le}\left(\frac{\partial \theta'}{\partial x_3} + \frac{\partial \Phi'}{\partial x_3}\right) - \left(\frac{2R_N}{Le}\right)\frac{\partial \theta'}{\partial x_3}. \tag{28}$$

In the linear theory of instability, all nonlinear terms in Eqs. (24)–(28), such as $u_i' \frac{\partial u_i'}{\partial x_j}$ or $\theta'\Phi'$, are neglected. In absence of nanoparticles, i.e., for regular fluids with $\phi_1 = \phi_0 = 0$, $D_B = 0$, $D_T = 0$, $d\bar{\Phi}/dX_3 = 0$, and $Le \sim 1/D_B \to \infty$, $N_{BT} = N_{TT} = 0$ and the term $-U_3'$ on the left hand site of Eq. (27) vanishes due to $d\bar{\Phi}/dX_3 = 0$. Eq. (27) thus becomes a zero identity, and Eqs. (24)–(26), (28) are reduced to the momentum and energy equations for free convection in regular fluids.

Eqs. (24)–(28) provide six equations to be solved for six unknowns: three velocity disturbances (U_i' for $i = 1$, 2, and 3), pressure disturbance (P'), temperature disturbance (θ'), and volumetric-fraction disturbance of nanoparticles (Φ'). To reduce the order of coupling among the six unknowns, U_1' and U_2' are eliminated from Eqs. (25) and (26). This results in the following equation for U_3' that are coupled with Φ' (Eq. (27)) and θ' (Eq. (28)):

$$\frac{\partial}{\partial \tau}\nabla^2 U_3' = Pr\nabla^4 U_3' - RaPr(\phi_1 - 1)\nabla_1^2\theta' - (\phi_0 - \phi_1)\{H\left[R_\rho - 1 + \beta(T_1 - T_0)\right]\nabla_1^2\Phi' + RaPr\left(\bar{\theta}\nabla_1^2\Phi' + \bar{\Phi}\nabla_1^2\theta'\right)\}, \tag{29}$$

where $\nabla^4 \equiv \partial^4/\partial x_1^4 + \partial^4/\partial x_2^4 + \partial^4/\partial x_3^4 + 2\partial^4/\partial x_1^2\partial x_2^2 + 2\partial^4/\partial x_2^2\partial x_3^2 + 2\partial^4/\partial x_1^2\partial x_3^2$ is the three-dimensional biharmonic operator, $\nabla^2 \equiv \partial^2/\partial x_1^2 + \partial^2/\partial x_2^2 + \partial^2/\partial x_3^2$ is the three-dimensional Laplacian operator, and $\nabla_1^2 \equiv \partial^2/\partial x_1^2 + \partial^2/\partial x_2^2$ is the two-dimensional Laplacian operator on the X_1–X_2 plane. Seeking for the convective cell patterns on the X_1–X_2 plane, with their intensities varying in the X_3-direction:

$$\begin{Bmatrix} \Phi'(X_1, X_2, X_3) \\ \theta'(X_1, X_2, X_3) \\ U_3'(X_1, X_2, X_3) \end{Bmatrix} = \mathrm{Exp}(\sigma\tau) f(X_1, X_2) \begin{Bmatrix} F(X_3) \\ \Theta(X_3) \\ U(X_3) \end{Bmatrix}, \tag{30}$$

the in-plan cell pattern, $f(X_1, X_2)$, is governed by

$$\nabla_1^2 f + a^2 f = 0, \quad \text{or} \quad \frac{\partial^2 f}{\partial X_1^2} + \frac{\partial^2 f}{\partial X_2^2} + a^2 f = 0, \tag{31}$$

with a being the reciprocal of the side-length of the convective cell, which is an unknown to be determined from the onset of instability. A close-form solution to Eq. (31) is [22],

$$f = \cos\left[\frac{a(\sqrt{3}X_1 + X_2)}{2}\right] + \cos\left[\frac{a(\sqrt{3}X_1 - X_2)}{2}\right] + \cos(aX_2), \tag{32}$$

which gives the hexagonal pattern in correspondence with the Bènard cells for regular fluids. The amplification rate of disturbances, σ in Eq. (30), is complex in nature, i.e., $\sigma = \sigma_r + i\sigma_i$ with $i = \sqrt{-1}$. The onset of instability is dictated by $\sigma_i = 0$, which separates the unstable regime ($\sigma_r > 0$) from the stable regime ($\sigma_r < 0$). Since we are not interested in the stable response represented by σ_i, under which the disturbances are sinusoidal and always stable, the onset of instability is represented by $\sigma = 0$, which is the same conditions used in studying the Bénard instability for regular fluids. Setting $\sigma = 0$ and substituting Eq. (30) into Eqs. (27)–(29), the equations governing the onset of instability are

$$F'' - a^2 F + R_N(\Theta'' - a^2\Theta) + \frac{U}{N_{BT}} = 0, \tag{33}$$

$$\Theta'' - \left(\frac{1 + 2R_N}{Le}\right)\Theta' - a^2\Theta - \frac{F'}{Le} = -U, \quad \text{and} \tag{34}$$

$$U'''' - 2a^2 U'' + a^4 U + a^2 Ra[(\phi_1 - 1) + (\phi_0 - \phi_1)\bar{\Phi}]\Theta + a^2(\phi_0 - \phi_1) \times \left\{\frac{Ra}{\beta(T_1 - T_0)}\left[R_\rho - 1 + \beta(T_1 - T_0)\right] + Ra\bar{\theta}\right\}F = 0, \tag{35}$$

with prime denoting differentiation with respect to X_3. The function U can be first eliminated from Eqs. (33) and (34):

$$F'' - a^2F + R_N(\Theta'' - a^2\Theta) = \frac{1}{N_{BT}}\left[\Theta'' - \left(\frac{1+2R_N}{Le}\right)\Theta' - a^2\Theta - \frac{F'}{Le}\right]. \quad (36)$$

Eq. (35) requires four boundary conditions for U, two at $X_3 = 0$ and two at $X_3 = 1$. For a rigid surface thereby [23], the non-slip condition and the continuity equation results in $U_3' = 0$ and $\partial U_3'/\partial X_3 = 0$, or $U = 0$ and $dU/dX_3 = 0$ according to Eq. (30). For a free surface where stress-free conditions apply, vanishing of the shear stresses tangent to the surface and continuity equation give $U_3' = 0$ and $\partial^2 U_3'/\partial X_3^2 = 0$, or $U = 0$ and $d^2U/dX_3^2 = 0$. A rigid (non-slip) boundary at $X_3 = 0$ and a free surface at $X_3 = 1$ will be considered to examine the effect of nanoparticle drifting. With the boundary values of $\bar\theta$ and $\bar\Phi$ absorbed in the primary flow, Eq. (18), the boundary conditions for θ' (Θ) and Φ' (F), and U_3' (U) in Eqs. (33)–(36) are thus,

$$\begin{aligned} &F = 0, \quad \Theta = 0, \quad U = 0, \quad U' = 0 \quad \text{at } X_3 = 0,\\ &F = 0, \quad \Theta = 0, \quad U = 0, \quad U'' = 0 \quad \text{at } X_3 = 1. \end{aligned} \quad (37)$$

Eqs. (35)–(37) display an eigenvalue problem for Ra, which is a function of a in correspondence with a specific size of the convection cells. To characterize the onset of instability, however, the smallest value of Ra, denoted by Ra_c and termed critical Rayleigh number, is targeted among all the possible values of a. Mathematically, this condition is represented by $d(Ra)/d(a) = 0$ for Ra_c to exist at a_c.

3. Eigenfunction expansions

A close form solution for the critical Rayleigh number will be attempted by the method of eigenfunction expansions in conjunction with the method of weighted residuals. The method has been shown highly accurate, within 0.4% as compared to the numerical solution by the use of only the first fundamental mode in the eigenfunction expansions for temperature.

3.1. Regular fluids

In absence of nanoparticles, small values for ϕ_0 and ϕ_1 are taken in Eqs. (34) and (35) to recover the case for regular fluids. Mathematically, $\phi_0 \to 0$, $\phi_1 \to 0$, and consequently $Le \to \infty$ according to Eq. (16). Eqs. (34) and (35) reduce to

$$\Theta'' - a^2\Theta = -U; \quad \Theta(0) = 0, \quad \Theta(1) = 0, \quad (38)$$

$$U'''' - 2a^2U'' + a^4U - a^2Ra\Theta = 0;$$
$$U(0) = 0, \quad U'(0) = 0, \quad U(1) = 0, \quad U''(1) = 0, \quad (39)$$

which are exactly the same governing equations for regular fluids [22,23]. Reciprocal of the cell size (a) and Rayleigh number (Ra) are the only parameters remained. Expanding Θ in terms of $\sin(m\pi X_3)$, which satisfy the boundary conditions in Eq. (38) and are orthogonal in the physical domain of $X_3 \in [0, 1]$,

$$\Theta(X_3) = \sum_{m=1}^{\infty} A_m \sin(m\pi X_3), \quad (40)$$

Eq. (39) can be solved for $U(X_3)$:

$$\begin{aligned} U(X_3) = \sum_{m=1}^{\infty} \frac{ae^{-aX_3}RaA_m}{2(e^{4a} - 4ae^{2a} - 1)\left[a^2 + (m\pi)^2\right]^2} \\ \times \{ \underset{①}{e^a} [\underset{②}{(e^{2a} - 1)(e^{2aX_3} - 1)(m\pi)^2(X_3 - 1)} \\ + 2a^3X_3(e^{2a} - e^{2aX_3}) + a^2[-1 + (X_3 - 1)e^{2a(1+X_3)} \\ + X_3 + (1 + 3X_3)(e^{2a} + e^{2aX_3})] + 2a[1 - e^{2a(1+X_3)} \\ + (1 + m^2\pi^2X_3)(e^{2a} - e^{2aX_3})]] \underset{②}{\sin(m\pi)} \\ - 2a [\underset{③}{m\pi} [\underset{④}{(X_3 - 2) \times (e^{2a(1+X_3)} - e^{2a})} \\ + X_3(e^{4a} - e^{2aX_3})] + e^{aX_3}(1 + 4ae^{2a} - e^{4a}) \\ \times \sin(m\pi X_3)] \} . \quad (41) \end{aligned}$$

Substituting Eq. (40) (for Θ) and Eq. (41) (for U) into Eq. (38) to form the residual, weighing the residual to zero by multiplying $\sin(n\pi X_3)$ on the residual, in turn, with $n = 1, 2, \ldots, m$, and integrating the results with respect to X_3 from 0 to 1, the results can be expressed in the following form:

$$\sum_{m=1}^{\infty} A_m b_{mn}(Ra, a) = 0, \quad n = 1, 2, \ldots, m;$$

$$\begin{aligned} b_{mn}(Ra, a) = \{ \underset{①}{-2m} [\underset{②}{2(a\pi)^3n(e^{2a} - 1)^2(m^2 - n^2)Ra} \\ + [\underset{③}{-2(a\pi)^2e^a(m^2 - n^2) \times [a^2(e^{2a} - 1)} \\ + a^3(e^{2a} + 1) + (n\pi)^2(a + ae^{2a} - e^{2a} + 1)]Ra \\ + (1 + 4ae^{2a} - e^{4a}) \times [a^2 + (n\pi)^2]^2[a^6 + 3(a^2m\pi)^2 \\ + (m\pi)^6 + a^2(3m^4\pi^4 - Ra)]\cos(m\pi)] \underset{③}{\sin(n\pi)}] \underset{②}{} \\ - \sin(m\pi) [\underset{④}{-2n(e^{4a} - 4ae^{2a} - 1)[a^2 + (m\pi)^2]^2} \\ \times [\underset{⑤}{a^6 + a^4(m^2 + 2n^2)\pi^2 + (mn^2\pi^3)^2} \\ + a^2[2(mn\pi^2)^2 + (n\pi)^4 - Ra]] \underset{⑤}{\cos(n\pi)} \\ - a\pi Ra(m^2 - n^2) \times [\underset{⑥}{-4an\pi \times e^a[(a^2 - m^2\pi^2)} \\ \times (e^{2a} - 1) + a(e^{2a} + 1)(a^2 + m^2\pi^2)] \\ + [\underset{⑦}{4a^6e^{2a} - (e^{2a} - 1)^2(mn\pi^2)^2} \\ + a^4\{3 + 3e^{4a} + 2e^{2a}[5 + 2\pi^2(m^2 + n^2)]\} \\ + (a\pi)^2 [\underset{⑧}{(e^{2a} - 1)^2n^2} \\ + m^2\{1 + e^{4a} + 2e^{2a} \times [2(n\pi)^2 - 1]\}]] \underset{⑧\ ⑦}{} \\ \times \sin(n\pi)]] \} / \{2\pi(e^{4a} - 4ae^{2a} - 1)(m^2 - n^2) \\ \times [a^2 + (m\pi)^2]^2[a^2 + (n\pi)^2]^2\}, \quad (42) \end{aligned}$$

where the paired brackets and braces are labeled for easier identifications. For nontrivial solutions of A_m at a prescribed value of m approximating Θ according to Eq. (40), the determinant of the coefficients must vanish, i.e., $|b_{mn}| = 0$, which gives the relation between Ra (Rayleigh number) and a (cell size) as the mth order solution. With $m = 1$ and $n = 1$ in Eq. (42), the first-order solution can be obtained,

$$\begin{aligned} b_{11} &= -\{\pi(a^2+\pi^2)^2(e^{4a}-4ae^{2a}-1)[a^6+3(a^2\pi)^2+\pi^6+a^2(3\pi^4-Ra)]+4Ra \\ &\quad\times(a\pi)^3(e^{2a}-1)^2\}/[2\pi(a^2+\pi^2)^4(e^{4a}-4ae^{2a}-1)]=0, \quad \text{or} \\ Ra &= \frac{(1+4ae^{2a}-e^{4a})(a^2+\pi^2)^5}{a^2\{[4a^3e^{2a}-a^2(e^{4a}-1)](a^2+2\pi^2)-\pi^4(e^{4a}-1)+4a\pi^2[1+e^{4a}+e^{2a}(\pi^2-2)]\}}. \end{aligned} \tag{43}$$

The critical cell size at the onset of instability is then determined from the condition

$$\begin{aligned} \left(\frac{dRa}{da}\right)_{a=a_c} &= 0, \quad \text{which gives } -32a^8e^{4a} \\ &\quad +8a^5e^{2a}(2a^2+5\pi^2)(e^{4a}-1)-3a^4(e^{2a} \\ &\quad -1)^2(e^{4a}+26e^{2a}+1)\pi^2+(e^{4a}-1)^2\pi^6 \\ &\quad +8a^2e^{2a}\pi^4[1+e^{4a}+2e^{2a}(\pi^2-1)] \\ &\quad +2a^3\pi^2(e^{4a}-1)[7+7e^{4a}+2e^{2a}(-7+4\pi^2)] \\ &\quad -2a\pi^4(e^{4a}-1)[3+3e^{4a}+e^{2a}(-6+4\pi^2)] \\ &\quad -2a^6[1+e^{8a}+e^{4a}(-2+24\pi^2)] \\ &= 0 \quad \text{at } a=a_c \Rightarrow a_c \cong 2.6824, \end{aligned} \tag{44}$$

which is exactly the same as the well-known result (2.682) obtained under the same boundary conditions [23]. Substituting the value of a_c into Eq. (43), $Ra_c \cong 1112.7$ is resulted, which is about 1% higher than the full (numerical) solution of 1100.65. High accuracy of the present approach is thus evident, by considering only the fundamental mode of $m = n = 1$. Should the second-order harmonics be attempted, $m = n = 2$, the same procedure results in $Ra_c \cong 1101.36$ (fundamental mode) and 21205.3 (second harmonics). The difference of the critical Rayleigh number from the full solution is rapidly reduced to 6.45×10^{-4}. The combined use of the eigenfunction expansion and weighted residual methods in Eqs. (40)–(42), in essence, is Trefftz's variational boundary method [24]. With all the boundary conditions satisfied in the eigenfunction expansions, the method is capable of capturing the fundamental eigenvalue (critical Rayleigh number) very accurately, usually by considering only the first eigenmode.

3.2. Nanofluids

In presence of Brownian motion and thermophoretic diffusion of nanoparticles in the fluid, the eigenfunction expansion for temperature, Eq. (40), remains the same. The modal response for the volume fraction of the nanoparticles, $F(X_3)$, results from solving Eq. (36) subject to the boundary conditions in Eq. (37). The result is

$$\begin{aligned} F(X_3) &= \sum_{m=1}^{\infty}[f_{1m}\cos(m\pi)+f_{2m}\sin(m\pi)+f_{3m}\sin(m\pi X_3) \\ &\quad +f_{4m}\cos(m\pi X_3)+f_{5m}], \end{aligned}$$

where

$$\begin{aligned} f_{1m} &= -4\left(g_1^{X_3}-1\right)\exp\left[(1-X_3)\left(\frac{1}{2LeN_{BT}}+\sqrt{g_1}\right)\right] \\ &\quad \times Le^3N_{BT}^2m\pi\left(a^2+m^2\pi^2\right)\times[1+N_{BT}(1+R_N)]/[g_2(g_1-1)], \\ f_{2m} &= -4\left(g_1^{X_3}-1\right)\exp\left[(1-X_3)\left(\frac{1}{2LeN_{BT}}+\sqrt{g_1}\right)\right](LeN_{BT})^2 \\ &\quad \times\left[Le^2N_{BT}\left(a^2+m^2\pi^2\right)^2-[LeN_{BT}(a^2+m^2\pi^2)]^2R_N\right. \\ &\quad \left.-m^2\pi^2(1+2R_N)\right]/[g_2(g_1-1)], \\ f_{3m} &= \{\left[Le\left(a^2+m^2\pi^2\right)\right]^2N_{BT}-\left[LeN_{BT}\left(a^2+m^2\pi^2\right)\right]^2R_N \\ &\quad -(m\pi)^2(1+2R_N)\}/\{(m\pi)^2+\left[LeN_{BT}\left(a^2+m^2\pi^2\right)\right]^2\}, \\ f_{4m} &= \frac{Le(a^2+m^2\pi^2)m\pi-[1+N_{BT}(1+R_N)]}{(m\pi)^2+[LeN_{BT}(a^2+m^2\pi^2)]^2}, \\ f_{5m} &= 4\left(g_1^{X_3}-g_1\right)\exp\left[-X_3\left(\frac{1}{2LeN_{BT}}+\sqrt{g_1}\right)\right] \\ &\quad \times Le^3N_{BT}^2m\pi\left(a^2+m^2\pi^2\right)[1+N_{BT}(1+R_N)]/[g_2(g_1-1)] \end{aligned} \tag{45}$$

with

$$g_1 = \exp\left[\frac{\sqrt{1+(2aLeN_{BT})^2}}{LeN_{BT}}\right],$$

$$g_2 = \left[1+2Le^2\left(a^2+m^2\pi^2\right)N_{BT}^2\right]^2-(2aLeN_{BT})^2-1.$$

Eq. (45) needs to be simplified to obtain a close form solution for the critical Rayleigh number. Noting that Le is of the order of 10^5 and (LeN_{BT}) is of the order of 10^5–10^6 [10], the long expression in Eq. (45) can be first expanded in terms of $1/Le$ and then the result in terms of $1/(LeN_{BT})$ to yield

$$\begin{aligned} F(X_3) &= \left(R_N-\frac{1}{N_{BT}}\right)\left(\frac{e^{-aX_3}}{e^{2a}-1}\right)\sum_{m=1}^{\infty}A_m\left[e^a\left(e^{2aX_3}-1\right)\right. \\ &\quad \left.\times\sin(m\pi)-e^{aX_3}\left(e^{2a}-1\right)\sin(m\pi X_3)\right]+O\left(\frac{1}{LeN_{BT}}\right). \end{aligned} \tag{46}$$

Eq. (40) (for $\Theta(X_3)$) and Eq. (46) (for $F(X_3)$) can now be substituted into Eqs. (35) and (37) to solve for $U(X_3)$. With $\Theta(X_3)$, $F(X_3)$, and $U(X_3)$ thus obtained, Eq. (34) is used to derive the residual. Following the same procedure for the case of regular fluids, multiplying the residual, in turn, by $\sin(n\pi X_3)$ with $n = 1,2,\ldots,m$, and integrating the result with respect to X_3 from 0 to 1, a similar expression to Eq. (42) can be obtained. The general expressions in this case, even with a greatly simplified expression for $F(X_3)$, become much more involved due to the tangling behaviors of Brownian motion and thermophoresis of nanoparticles.

4. First-order approximation

The first-order approximation with $m = 1$ in Eq. (40), evidenced by the case of regular fluids in Eq. (43), is expected to yield a close approximation to the critical Rayleigh number for the case of nanofluids. With $\Theta = A_1\sin[\pi X_3]$, $F(X_3)$ in Eq. (46) becomes

$$F(X_3) = A_1\left(\frac{1}{N_{BT}} - R_N\right)\sin[\pi X_3], \quad \text{and consequently,}$$
$$F'(X_3) \cong A_1\left(\frac{1}{N_{BT}} - R_N\right)\pi\cos[\pi X_3]. \tag{47}$$

With $(LeN_{BT}) \sim 10^5$, accuracy of Eq. (47) is on the order of 10^{-5}. With practical properties of nanofluids, Eq. (47) will be shown indistinguishable from the general solution in the numerical examples. The residual of Eq. (34) can now be calculated by integrating Eq. (35) for $U(X_3)$, with the boundary conditions in Eq. (37). Weighing the residual by $\sin[\pi X_3]$ in integrating the result from 0 to 1, diminution of the coefficient of A_1, $b_{11} = 0$ in correspondence with Eq. (43) results in

$$\begin{aligned}
Ra = {} & 2(a^2+\pi^2)^6(e^{4a} - 4ae^{2a} - 1)N_{BT}\beta(T_0 - T_1) \\
& / \underset{①}{\{}\, a^2(\phi_0 - \phi_1) \underset{②}{[} -2(a^2+\pi^2) \\
& \times \{4a^3e^{2a}(a^2+2\pi^2) - (e^{4a}-1)(a^2+\pi^2)^2 \\
& + 4a\pi^2[1 + e^{4a} + e^{2a}(-2+\pi^2)]\} \\
& + \beta(T_0 - T_1) \underset{③}{[} -4a^5e^{2a}(a^2+3\pi^2) + a^4(e^{4a}-1) \\
& \times (a^2+3\pi^2) + 3(a\pi)^2(e^{2a}-1) \times [-8 - 16e^a \\
& + \pi^2 + e^{2a}(-8+\pi^2)] - 4\pi^4 ae^a[4 + 4e^{2a} + e^a(8+\pi^2)] \\
& + (e^{2a}-1)\pi^4 \times [8 + 16e^a + \pi^2 + e^{2a}(8+\pi^2)] \\
& - 4a^3\pi^2e^a[4 + 4e^{2a} + e^a(8+3\pi^2)] + N_{BT} \\
& \times \underset{④}{[}\, 4a^7e^{2a} - a^6(e^{4a}-1) + 12\pi^2a^5e^{2a} - 3(a^2\pi)^2(e^{4a}-1) \\
& + 4a\pi^4[2 - 4e^a - 4e^{3a} + 2e^{4a} + e^{2a}(\pi^2 - 12)] \\
& - \pi^4(e^{2a}-1)[-8 - 16e^a + \pi^2 + e^{2a}(\pi^2 - 8)] \\
& + 4a^3\pi^2[2 - 4e^a - 4e^{3a} + 2e^{4a} + 3e^{2a}(\pi^2 - 4)] \\
& - 3(a\pi)^2(e^{2a}-1)[8 + 16e^a + \pi^2 + e^{2a}(8+\pi^2)] \\
& + \underset{⑤}{[}\, 4a^7e^{2a} - a^6(e^{4a}-1) + 12a^5\pi^2e^{2a} - 3(a^2\pi)^2(e^{4a}-1) \\
& - 3(a\pi)^2(e^{2a}-1) \times [-8 - 16e^a + \pi^2 + e^{2a}(\pi^2 - 8)] \\
& + 4a\pi^4e^a[4 + 4e^{2a} + e^a(\pi^2+8)] - (e^{2a}-1)\pi^4 \\
& \times [8 + 16e^a + \pi^2 + e^{2a}(8+\pi^2)] + 4a^3\pi^2e^a \\
& \times [4 + 4e^{2a} + e^a(3\pi^2+8)] \underset{⑤}{]}\, R_N \underset{④}{]}\, \underset{③}{]}\, -2(a^2+\pi^2) \\
& \times [N_{BT}R_N(R_\rho - 1) + R_\rho]\{4a^3e^{2a}(a^2+2\pi^2) \\
& - (a^2+\pi^2)^2(e^{4a}-1) + 4a\pi^2 \times [1 + e^{4a} + e^{2a}(\pi^2-2)]\} \underset{②}{]} \\
& + 2(a^2+\pi^2)\{4a^3e^{2a}(a^2+2\pi^2) - (a^2+\pi^2)^2(e^{4a}-1) \\
& + 4a\pi^2[1 + e^{4a} + e^{2a}(\pi^2-2)]\} \\
& \times N_{BT}\beta(T_0 - T_1)(-1+\phi_1)\,\underset{①}{\}}
\end{aligned} \tag{48}$$

The last term containing $(-1+\phi_1)$ has been singled out intentionally. To preserve the novelty observed in nanofluids, the value of ϕ_1 needs to be less than a few percent [1]. With ϕ_1 on the order of 10^{-2}, the factor $(-1+\phi_1)$ in the denominator of Eq. (48) can be replaced by -1 without causing too much error. The Rayleigh number, with the term containing ϕ_1 ignored, is a function of the cell-size parameter (a), the temperature difference $(T_1 - T_0)$, the volume-fraction *difference* of nanoparticles $(\phi_0 - \phi_1)$, the thermal expansion coefficient (β) of the nanofluids, the density ratio (R_ρ), and the two nondimensional parameters N_{BT} and R_N. Note that the Rayleigh number is no longer a function of Lewis number (Le), which was dropped in the first-order approximation for $F(X_3)$, Eq. (47).

The Rayleigh number given by Eq. (48) reduces to that in Eq. (43) for regular fluid. In the limit of $\Delta\phi = (\phi_0 - \phi_1) \to 0$, including the case of $\phi_0 = 0$ and $\phi_1 = 0$ (no nanoparticle), effects of thermophoresis and Brownian motion of nanoparticles disappear and the Rayleigh number for regular fluids is perfectly recovered. The quantities grouped within bracket no. 2 in Eq. (48), therefore, reflect the combined effects of thermophoresis and Brownian motion of nanoparticles in presence of a concentration gradient.

The limit of $\Delta\phi \to 0$ plays an important role in determining the critical dimension of the convective cells (a_c). Since the volume fractions of nanoparticles, both ϕ_0 and ϕ_1, are usually less than a few percent [1–5] to preserve the novel behavior of nanofluids, the difference between ϕ_0 and ϕ_1 is indeed very small in practice. As far as the value of a_c is concerned, therefore, its value should be very close to that determined from the limit of $\Delta\phi = \phi_0 - \phi_1$ approaching zero. The Rayleigh number given by Eq. (48) reduces to that in Eq. (43) in the limit of $\Delta\phi \to 0$. The critical condition of $d(Ra)/da = 0$ at $a = a_c$ from Eq. (48), in the limit of $\Delta\phi \to 0$, consequently, is identical to Eq. (44). The resulting $a_c \cong 2.6824$ is expected to hold for nanofluids as well, with ϕ_0 and ϕ_1 being less than a few percent. With a replaced by 2.6824 in Eq. (48),

$$Ra_c = -2100.05 N_{BT}\beta(T_0 - T_1)/\underset{①}{\{}[1.887(R_\rho - 1) - \beta(T_0 - T_1)](\phi_0 - \phi_1) + N_{BT}\{-1.887R_N(R_\rho - 1) \times (\phi_0 - \phi_1) + \beta(T_0 - T_1)[(0.887 + R_N) \times (\phi_0 - \phi_1) - 1.887]\}\underset{①}{\}}, \quad (49)$$

while the value of a_c is *independent* of the properties of nanofluids, which will be proven in the numerical examples below based on the general result shown by Eq. (48), the value of Ra_c depends on $\beta(T_0 - T_1)$, $(\phi_0 - \phi_1)$, N_{BT}, R_ρ, and R_N.

4.1. Other boundary conditions

Eqs. (48) and (49) were derived for nanofluids between a rigid (non-slip) and a free surface, $U = 0$ and $U' = 0$ at $X_3 = 0$ and $U = 0$ and $U'' = 0$ at $X_3 = 1$, as described in Eq. (37). This condition simulates the thin-film region between a bubble and a hot surface as illustrated at the bottom in Fig. 1. Other possible combinations are rigid bounding surfaces, upper left in Fig. 1, where the non-slip conditions apply, $U = 0$ and $U' = 0$ at both $X_3 = 0$ and 1, and free–free surfaces, upper right in Fig. 1, where the stress-free condition ($U = 0$ and $U'' = 0$) applies at both $X_3 = 0$ and 1.

Replacing the boundary conditions in Eq. (37) accordingly, the critical Rayleigh number under the various surface conditions can be determined in exactly the same way. The first-order ($m = 1$) solutions are

Rigid–rigid surfaces: $a_c \cong 3.11421$ and

$$Ra_c = -3430.16 N_{BT}\beta(T_0 - T_1)/\underset{①}{\{}[2(R_\rho - 1) - \beta(T_0 - T_1)](\phi_0 - \phi_1) + N_{BT}\{-2R_N(R_\rho - 1) \times (\phi_0 - \phi_1) + \beta(T_0 - T_1)[R_N(\phi_0 - \phi_1) - 2]\}\underset{①}{\}}. \quad (50)$$

Free–free surfaces: $a_c \cong 2.22144$ and

$$Ra_c = -27\pi^4 N_{BT}\beta(T_0 - T_1)/\underset{①}{\{}2\underset{②}{[}[2(R_\rho - 1) - \beta(T_0 - T_1)](\phi_0 - \phi_1) + N_{BT}\{-2R_N(R_\rho - 1) \times (\phi_0 - \phi_1) + \beta(T_0 - T_1)[(1 + R_N)(\phi_0 - \phi_1) - 2]\}\underset{②}{]}\underset{①}{\}}. \quad (51)$$

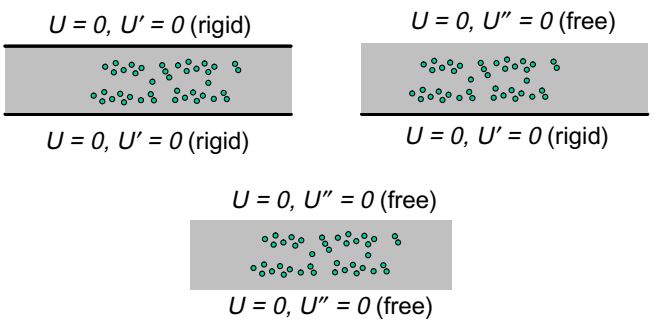

Fig. 1. The various surfaces bounding the nanofluids.

The present case with a rigid (at $X_3 = 0$) and a free ($X_3 = 1$) surface is the most complicated among the three, and hence having the longest expression for the Rayleigh number, due to the non-symmetrical boundary conditions at $X_3 = 0$ and 1. Under the same conditions, the critical Rayleigh number is the highest (lowest), and hence most stable (unstable), for the case of rigid–rigid (free–free) surfaces. The case of rigid-free surfaces is between the two.

The critical Rayleigh number shown in Eqs. (49)–(51) depends on density (through R_ρ and D_T), heat capacity (through α in N_{BT}), thermal conductivity (through α in N_{BT} and k in D_T), and viscosity (through D_T and D_B) of the nanofluid. Because they are also involved in the coefficients of Eqs. (10)–(15), heat transfer coefficient (Nusselt number) derived from integrating Eqs. (10)–(15) will also depend on these properties.

5. Results and discussion

Validity of Eq. (47) is a key to obtain the close form solution of the Rayleigh number. For the fundamental mode with $m = 1$, based on which the close form solutions are derived in Eqs. (48) and (49), Fig. 2 compares the full expression of $F(z)$ shown by Eq. (45) and the approximate solution shown by Eq. (47). For $N_{BT} = 0.2$, a typical value for alumina/water nanofluids as shown in Fig. 2(a), the full

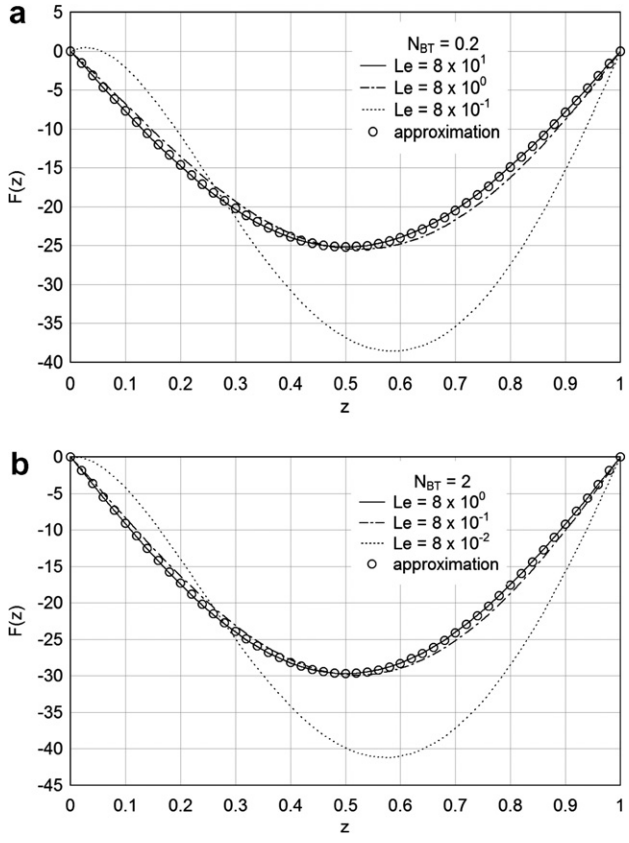

Fig. 2. Comparisons of the fundamental mode ($m = 1$) for $F(z)$: Full expression shown by Eq. (45) and approximate expression shown by Eq. (47).

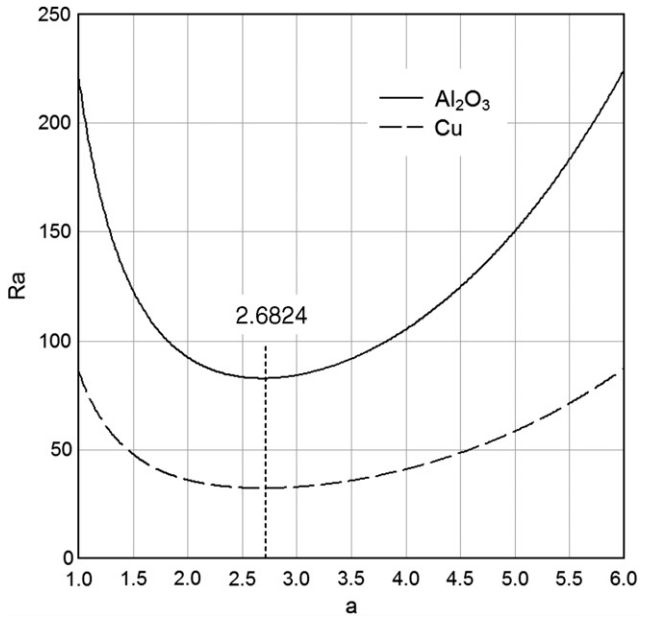

Fig. 3. Water-based nanofluids with alumina and copper nanoparticles with $\Delta T = 10$ K and $\Delta\phi = 1$ vol%. Al_2O_3: $\beta = 6 \times 10^{-3}$, $Le = 8 \times 10^5$, $N_{BT} = 0.2$, $R_\rho = 4$, $R_N = 30.18$; Cu: $\beta = 6 \times 10^{-4}$, $Le = 7 \times 10^5$, $N_{BT} = 2$, $R_\rho = 9$, $R_N = 3.018$. Critical Rayleigh number occurs at $a_c = 2.6824$.

expression becomes indistinguishable from the approximate solution as the value of Le increases beyond 8×10^1. For $Le \cong 8 \times 10^5$ in alumina/water nanofluids, which is four orders of magnitude greater, the approximate expression becomes exact. The same behavior is observed for copper/water nanofluids with $N_{BT} = 2$, Fig. 2(b). No sensible difference between the full and approximate expressions can be observed beyond $Le \sim 8 \times 10^0$, as compared to $Le \cong 7 \times 10^5$ for copper/water nanofluids. Eq. (47), therefore, is indeed a very close approximation to the full solution shown by Eq. (45).

Fig. 3 compares the stability curves for water based nanofluids with alumina and copper nanoparticles. Thermofluid properties are calculated based on 10 nm nanoparticles, which are summarized in the figure caption. In spite of the uncertainty in the extended use of N_T in Eq. (5) for nanoparticles, the value of R_N should be of the order of 10^0–10^2 for nanoparticles in the range of 1–100 nm. The value of R_N for copper is reduced by one order of magnitude from that for alumina because thermal conductivity of copper is about one order of magnitude higher than that of alumina. Eq. (48) is used in producing Fig. 3.

The critical value of Rayleigh number (Ra_c) occurs at $a_c = 2.6824$ in both cases, as proven analytically above, regardless of the different thermophysical properties in different nanofluids. The value of Ra_c is lowered by two orders of magnitude, 82.7172 for the alumina/water nanofluid and 32.2006 for the copper/water nanofluid, as compared to $Ra_c \cong 1112.7$ for the regular fluid without nanoparticle. In terms of the higher value of Ra_c at the onset of instability, alumina/water nanofluid is more stable than the copper/water nanofluid.

The close form solution of the Rayleigh number obtained in Eq. (48) makes it convenient to illustrate the various effects involved. Threshold values for water nanofluids with metallic/metallic oxide nanoparticles of 1–100 nm are used in the numerical examples: $R_N = 30.18$, $N_{BT} = 0.2$, $Le = 8 \times 10^5$, and $\beta = 5.32 \times 10^{-4}$. The value of $R_\rho = 6$ is taken from the mean between 4 (aluminum nanoparticles) and 9 (copper nanoparticles). The values of ΔT and $\Delta\phi$ are taken as 80 K and 1 vol%, respectively, unless stated otherwise. Fig. 4 shows that the critical Rayleigh number decreases as (a) the temperature difference $\Delta T = T_0 - T_1$ decreases, (b) the volume-fraction difference of nanoparticles, $\Delta\phi = \phi_0 - \phi_1$, increases, (c) the density ratio R_ρ increases, (d) the ratio R_N increases, and (e) the value of N_{BT} increases. In terms of the lower value of the critical Rayleigh number, these are the destabilizing effects for natural convection in nanofluids. The critical value of Rayleigh number (Ra_c) remains to occur at $a_c = 2.6824$ in all cases and, depending on the thermophysical properties of the nanofluids, the critical Rayleigh number can be lowered than that of the regular fluid by two orders of magnitude. A larger temperature difference (ΔT) produces a larger buoyancy force, which effectively suppresses the temporal growth of the disturbances and consequently results in a more stable behavior as shown in Fig. 4(a). Brownian motion of the nanoparticles is promoted as the difference of the volume fraction of nanoparticles ($\Delta\phi$) increases. This is a destabilizing effect, as shown by Fig. 4(b), in terms of a much lower value of Ra_c now only of the order of 10^0–10^1. With other conditions remained the same, effect of R_ρ shown by Fig. 4(c), heavier nanoparticles moving through the base fluid produce stronger disturbances. It thus facilitates development of turbulence, resulting in a lower critical Rayleigh number at a larger value of R_ρ. Fig. 4(d) shows that the critical value of Ra_c decreases as the ratio of R_N increases. While both thermophoresis and Brownian motion are driving forces in support of the motion of nanoparticles, thermophoresis at a higher value of thermophoretic diffusivity is more favorable to the initiation of turbulence in nanofluids. Though not as strong as thermophoresis, Brownian motion also promotes turbulence in nanofluids, as shown in Fig. 4(e). The critical Rayleigh number is smaller for nanofluids with a larger value of the Brownian diffusion coefficient. Note that the case of $N_{BT} = 2$ shown in Fig. 4(e) has already approached the lower bound of $N_{BT} \to \infty$. From Eq. (48),

$$\lim_{N_{BT}\to\infty} Ra = -\frac{2(a^2+\pi^2)^3\beta(T_0-T_1)}{a^2[-2R_N(R_\rho-1)(\phi_0-\phi_1)+\beta(T_0-T_1)[(1+R_N)(\phi_0-\phi_1)-2]}, \tag{52}$$

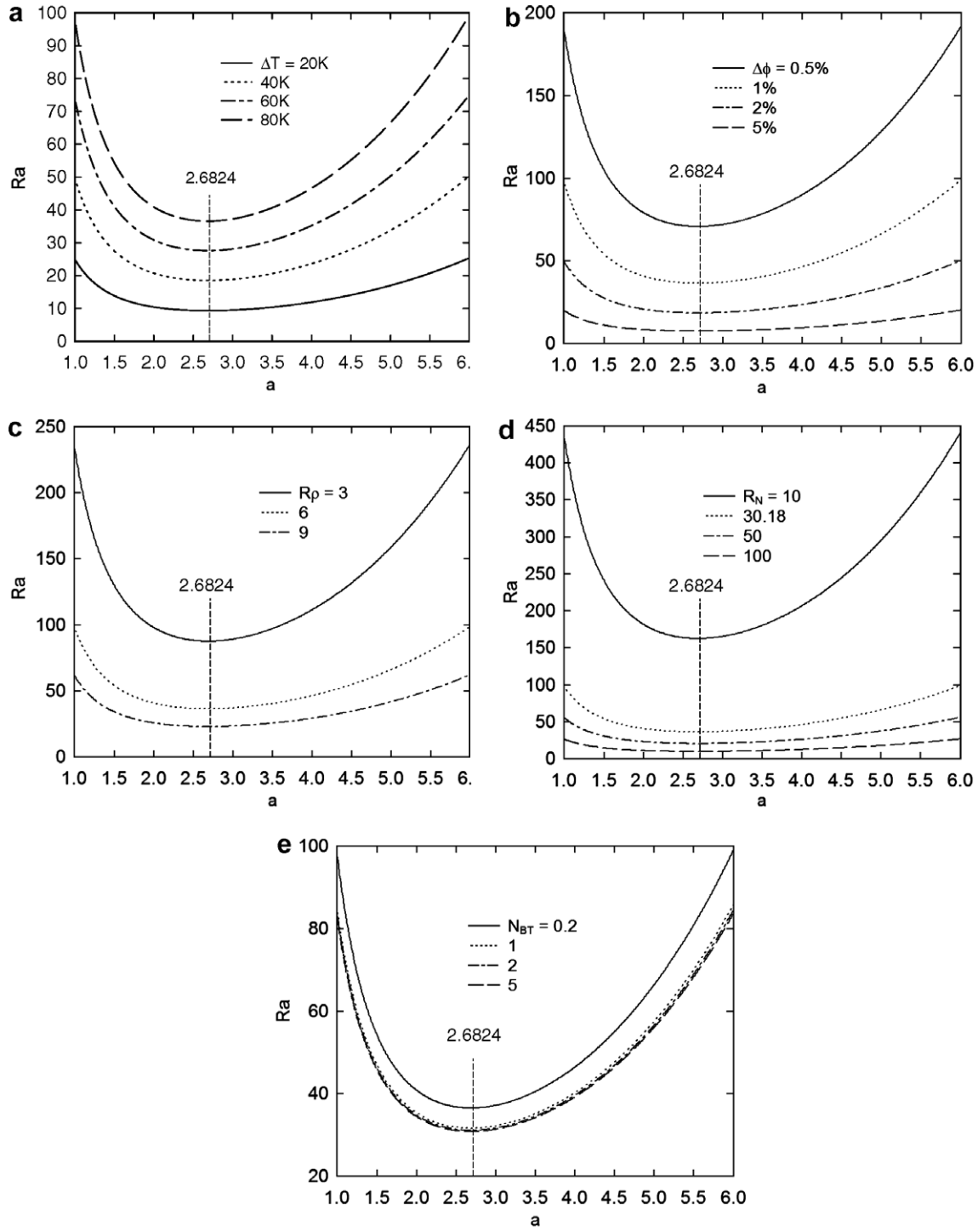

Fig. 4. Effects of (a) $\Delta T = T_0 - T_1$, (b) $\Delta\phi = \phi_0 - \phi_1$, (c) R_ρ, (d) R_N, and (e) N_{BT} on the Rayleigh number (Ra): $a_c = 2.6824$ in all cases.

with the same parameters used in Fig. 4, $Ra_c \cong 30.6604$ as $N_{BT} \to \infty$, which is the value of Ra_c at $a_c = 2.6824$ shown in Fig. 4(e).

The critical Rayleigh number (Ra_c) for the case of $\Delta T = 80$ K in Fig. 4(a) is 36.5496, resulting from the use of $m = 1$ in Eqs. (40) and (46), which is the base for comparison as other parameters are varied in Fig. 4. The corresponding values of Ra_c for $m = 2$ and 3, respectively, are 36.1804 and 36.1599, showing an accuracy of about 1% captured by the first-order ($m = 1$) solution. The second and third harmonics are $Ra_c \cong 685.382$ for $m = 2$ and $Ra_c \cong 5550.12$ for $m = 3$. The combined use of the eigenfunction expansion method and the weighted residual method in this work does provide a highly accurate approach as far as the critical Rayleigh number (eigenvalues) is concerned.

In correspondence with $a_c \cong 2.6824$ and $Ra_c \cong 36.5496$ for rigid-free surfaces, under the same conditions, the critical conditions for the case of rigid–rigid surfaces are $a_c \cong 3.11421$ and $Ra_c \cong 56.3136$ (Eq. (50)) and those for the case of free–free surfaces are $a_c \cong 2.22144$ and $Ra_c \cong 21.5925$ (Eq. (51)). Comparing to the corresponding cases for regular fluids [23], $a_c \cong 3.117$ and $Ra_c \cong 1707.762$ (rigid–rigid) and $a_c \cong 2.2214$ and $Ra_c \cong 657.511$ (free–free), the length parameter at the onset of instability (a_c) stays the same while the critical Rayleigh number is again lowered by one order of magnitude due to the combined behavior of Brownian motion and thermophoresis of nanoparticles. Highly promoted turbulence in nanofluid enhances the overall heat transfer coefficient, which is a key to understand the nearly uniform temperature across the vaporization/condensation sections in oscillating heat pipes subjected to high heat-flux [25].

The present work focuses on the critical point separating the laminar and the turbulent regimes. Determination of the Nusselt number is the most important task to follow, after the onset of instability is determined from the critical Rayleigh number (Ra_c) derived in Eqs. (49)–(51). Different sets of mass, momentum, and energy equations need to be integrated in different regimes of the Rayleigh number; namely in the laminar regime for $Ra < Ra_c$ or in the turbulent regime for $Ra > Ra_c$, which will be a major task by itself. In the simplest case for a nanofluid passing over a hot surface, in addition to the classical Reynold's and Prandtl numbers, six dominant parameters have shown in the expression for the Nusselt number. All details will be reported in our future communication [26].

6. Conclusion

Instability of natural convection for nanofluids between two plates, heated from below, is studied in this work. The combined behavior of Brownian motion and thermophoresis of nanoparticles is shown to provide a strong destabilizing effect, which reduces the critical Rayleigh number by as much as two orders of magnitude as compared to that of the regular fluids without nanoparticles. The much lower critical Rayleigh number suggests that turbulence may be the dominating mode for natural convection in most nanofluids. The critical Rayleigh number depends on the differences of temperature ($T_0 - T_1$) and volume concentration ($\phi_0 - \phi_1$) between the two plates, as well as the thermal expansion coefficient of the nanofluids (β), the density ratio of the nanoparticle to the base fluid (R_ρ), the Brownian-to-thermal-diffusivity ratio (N_{BT}), and the Brownian-motion-to-thermophoretic diffusivity ratio (R_N). Lewis number (Le) does appear in natural convection, but it is a high-order effect as compared to others at the onset of instability. The critical Rayleigh number is not a function of Le.

Close form solutions for the Rayleigh number have been established to resolve the nanoparticle effect. For nanofluids between two free surfaces, Brownian motion and thermophoresis of nanoparticles do not change the geometrical configuration of the convective cell. At the onset of instability for nanofluid bounded by a rigid and a free surface, the critical value of a_c stays approximately at 2.6824, which is independent of the nanofluid properties. In general, the presence of nanoparticles does not affect the critical cell size at the onset of instability, regardless of the surface conditions involved. As compared to the rigid–rigid ($Ra_c \cong 56.3136$ at $a_c \cong 3.11421$) and free–free ($Ra_c \cong 21.5925$ at $a_c \cong 2.22144$) surface conditions, the critical Rayleigh number for the case of rigid-free surfaces ($Ra_c \cong 36.5496$ at $a_c \cong 2.6824$) is between the two. The constraints imposed on the growth of disturbances are not as strong as those in the case of rigid–rigid surfaces, but are weaker than those in the case of free–free surfaces. The analysis has been conducted by assuming constant thermal properties of nanofluids. Drastic reductions of the critical Rayleigh number, consequently, should be viewed qualitative for the time being. The property enhancements by nanoparticles have been challenged by recent studies, but it remains to be worthwhile to instate the volume-fraction dependent thermal properties in the analysis and reexamine the drastic reductions of Ra_c obtained in this work. Close form solutions, however, will not be possible in this extension due to the stiff nonlinearity of the problem.

Heat transfer enhancement by nanoparticles can be more than an increase of the effective thermal conductivity alone. Dominance of turbulence shown in this work, in terms of the much lower critical Rayleigh number by one to two orders of magnitude, should be explanatory for the superior performance of oscillating heat pipes employing nanofluids.

References

[1] J.A. Eastman, S.U.S. Choi, S. Li, W. Yu, L.J. Thompson, Anomalously increased effective thermal conductivities of ethylene glycol-based nanofluids containing copper nanoparticles, Appl. Phys. Lett. 6 (2001) 718–720.
[2] S. Lee, S.U.S. Choi, J.A. Eastman, Measuring thermal conductivity of fluids containing oxide nanoparticles, ASME J. Heat Transfer 121 (1999) 280–289.
[3] Y. Xuan, Q. Li, Heat transfer enhancement of nanofluids, Int. J. Heat Mass Transfer 21 (2000) 58–64.
[4] S.U.S. Choi, Z.G. Zhang, W. Yu, F.E. Lockwood, E.A. Grulke, Anomalous thermal conductivity enhancement in nanotube suspensions, Appl. Phys. Lett. 79 (2001) 2252–2254.
[5] S.K. Das, N. Putra, P. Thiesen, W. Roetzel, Temperature dependence of thermal conductivity enhancement for nanofluids, ASME J. Heat Transfer 125 (2003) 567–574.
[6] B.C. Pak, Y. Cho, Hydrodynamics and heat transfer study of dispersed fluids with submicron metallic oxide particles, Exp. Heat Transfer 11 (1998) 151–170.
[7] Y. Xuan, Q. Li, Investigation of convective heat transfer and flow features of nanofluids, ASME J. Heat Transfer 125 (2003) 151–155.
[8] Y. Xuan, W. Roetzel, Conceptions for heat transfer correlation of nanofluids, Int. J. Heat Mass Transfer 43 (2000) 3701–3707.
[9] S. Maïga, C.T. Nguyen, N. Galanis, G. Roy, Heat transfer behaviors of nanofluids under in a uniformly heated tube, Superlattices Microstruct. 35 (2004) 543–557.

[10] J. Buongiorno, Convective transport in nanofluids, ASME J. Heat Transfer 128 (2006) 240–250.
[11] W. Yu, S.U.S. Choi, The role of interfacial layers in the enhanced thermal conductivity: A renovated Maxwell model, J. Nanopart. Res. 5 (2003) 167–171.
[12] S.P. Jang, S.U.S. Choi, Role of Brownian motion in the enhanced thermal conductivity of nanofluids, Appl. Phys. Lett. 84 (2004) 4316–4318.
[13] D.H. Kumar, H.E. Patel, Rajeev Kumar, J. Sundararajan, T. Pradeep, S.K. Das, Model for heat conduction in nanofluids, Phys. Rev. Lett. 93 (2004) 144301.
[14] G. Chen, Ballistic-diffusive heat-conduction equation, Phys. Rev. Lett. 86 (2001) 2297–2300.
[15] P. Keblinski, S.R. Phillpot, S.U.S. Choi, J.A. Eastman, Mechanisms of heat flow in suspensions of nano-sized particles (nanofluids), Int. J. Heat Mass Transfer 45 (2002) 855–863.
[16] P. Vadasz, Heat conduction in nanofluid suspensions, ASME J. Heat Transfer 128 (2006) 465–477.
[17] G. Polidori, S. Fohanno, C.T. Nguyen, A note on heat transfer modeling of Newtonian nanofluids in laminar free convection, Int. J. Therm. Sci. 46 (2007) 739–744.
[18] G.S. McNab, A. Meisen, Thermophoresis in liquids, J. Colloid Interf. Sci. 44 (1973) 339–346.
[19] S.P. Jang, U.S.U. Choi, Free convection in a rectangular cavity (Bénard convection) with nanofluids, Proc. 2004 IMECE, Anaheim, California, November 13–20 (2004).
[20] P. Keblinski, D.G. Cahill, Comment on model for heat conduction in nanofluids, Phys. Rev. Lett. 95 (2005) 209401.
[21] S.A. Putnam, D.G. Cahill, P.V. Braun, Thermal conductivity of nanoparticle suspensions, J. Appl. Phys. 99 (2006) 084308.
[22] C.S. Yih, Fluid Mechanics – A Concise Introduction to the Theory, West River Press, Ann Arbor, Michigan, 1977 (Chapter 9).
[23] S. Chandrasekhar, Hydrodynamic and Hydromagnetic Stability, Oxford University Press, Oxford, England, 1961, Chapter II.
[24] B.A. Finlayson, The Method of Weighted Residuals and Variational Principles, Academic Press, New York, 1972.
[25] H.B. Ma, C. Wilson, Q. Yu, U.S. Choi, M. Tirumala, An experimental investigation of heat transport capability in a nanofluid oscillating heat pipe, ASME J. Heat Transfer 128 (2006) 1213–1216.
[26] E.J. Pfautsch, Heat transfer of nanofluids – External flow over a hot surface, MS Thesis, University of Missouri, Columbia, MO, 2007.